6. MAGNETIC ANALYSIS

A general description of the iron yoke, including the main dimensions, is given in Chapt. 3. Detailed constructional descriptions are given in Chapt. 7 for the barrel section, and in Chapt. 8 for the endcap sections. This chapter is only concerned with the description of the field map, including the stray field, and the forces associated with the magnetic field, both on ferromagnetic elements and on currents.

An important issue is the computation of the forces due to any asymmetry in the system, such as misalignment of the coil inside the yoke, asymmetry of the yoke itself and the coil chimney cut-outs, or an inhomogeneous magnetic permeability distribution.

6.1 GEOMETRY OF THE IRON YOKE

The following is a description of all the ferromagnetic components of the magnet yoke as it has been used for the magnetic computation (Fig. 6.1).

Some discrepancies, at the level of a few cm, may be noticed with reference to the actual CMS parameter drawings, because of recent evolution in subdetector geometries. The official and most up to date dimensions will always be accessible through WWW, as explained in Chapt. 5.

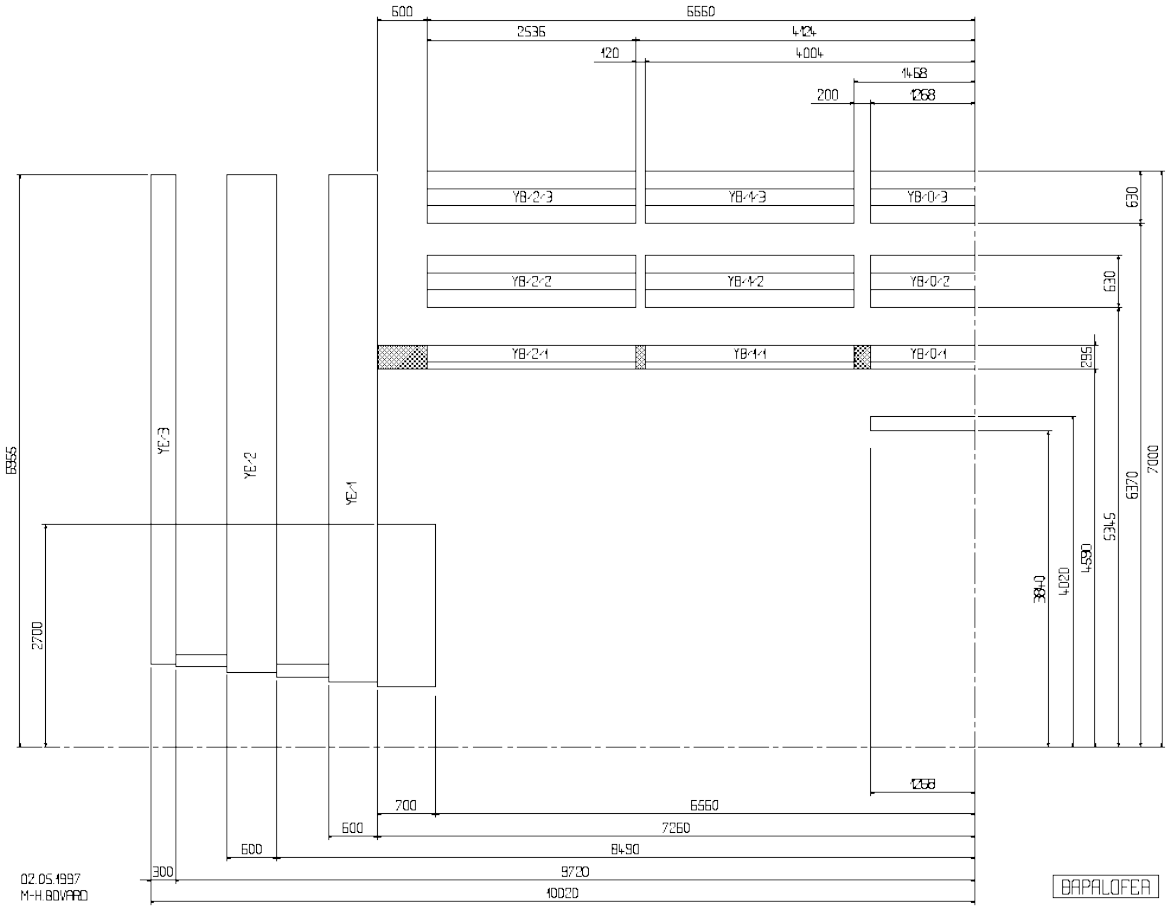

Fig. 6.1: Geometrical description of the magnet yoke used for the magnetic computations.

The innermost iron layer starts at R = 4590 mm on flats, and the outermost (the third

one), ends at R = 7000 mm (on flats).

Successive overall thickness of layers are T_1 = 295 mm, T_2 = 630 mm and T_3 = 630 mm.

It should be noted that the blocks of all three layers could either be made of sandwiched plates or be monoblock (rolled and/or forged).

In the former case, the inner layer blocks are composed of two plates having their matching faces fully machined while the second and third layer blocks may present, due to the tolerances of fabrication, a gap between their three constitutive plates. These plates will be machined only at the bolting points so as to be precisely assembled using calibrated washers, thus avoiding machining of large surfaces.

The fabrication tolerance of the plate thickness is required to be +0/-10 mm; consequently, as far as magnetic material is concerned, the real minimum thickness of the inner layer blocks could be 285 mm whereas the real minimum thickness of second and third layer blocks could be only 600 mm. This pessimistic situation has been taken into account for all the subsequent calculations.

The central ring YB0 is separated from the two adjacent ‘first outside rings’ by gaps of 200 mm, whereas the gaps separating the ‘first outside rings’ from the ‘second outside rings’ are only 120 mm.

It may be possible to reduce the two 200 mm gaps to 150 mm to increase the muon acceptance; this would also have a positive effect in reducing the stray field.

Connecting brackets, in normal construction steel, join the steel plates forming together the three layers and provide the geometry and the required structural rigidity.

Both endcap yokes are composed of three 13.9 m diameter disks (across flats). The two innermost disks are 600 mm thick and the outermost 300 mm (maybe later 250 mm). The inner disk is separated from the adjacent barrel ring by 600 mm, and all disks are equally spaced by 600 mm to accommodate the endcap muon chambers. A supplementary disk, 5 m in diameter and 250 mm thick, which serves as interface for the radiation shielding surrounding the HF calorimeter, has been added at a distance of 600 mm from the outermost large disk. Attached to the innermost disk, and facing the interaction point, is a solid iron piece 5.4 m in diameter and 700 mm thick called the nose, (YN). The total thickness of magnetic material in the nose is in fact 800 mm, as 100 mm are incorporated in the hadronic endcap calorimeter, (HE). Finally, some iron shielding rings are mounted on the inner diameter of each disk so as to rest against the preceding one when in the closed operational position. A mean radial thickness of 150 mm for these rings has been assumed for the magnetic computations.

6.2 MAGNETIC MODEL AND INPUTS

Computations have been made at CERN using the POISSON code program, at CEA Saclay using CASTEM code [6-2, 6-3], and at INFN Genova [6-4] and Wisconsin University [6-1], both using ANSYS code. All are 2-dimensional axisymmetric programs, thus needing to approximate the section of the return area from a regular 12-sided polygon to a cylinder. This may have been done in slightly different ways from one place to another but the effect is second order to negligible on the global results.

The B-H curve used for most computations have been derived from actual

measurements done on construction steel, delivered from Russia and France, for the construction of the L3 magnet (see Fig. 6.2).

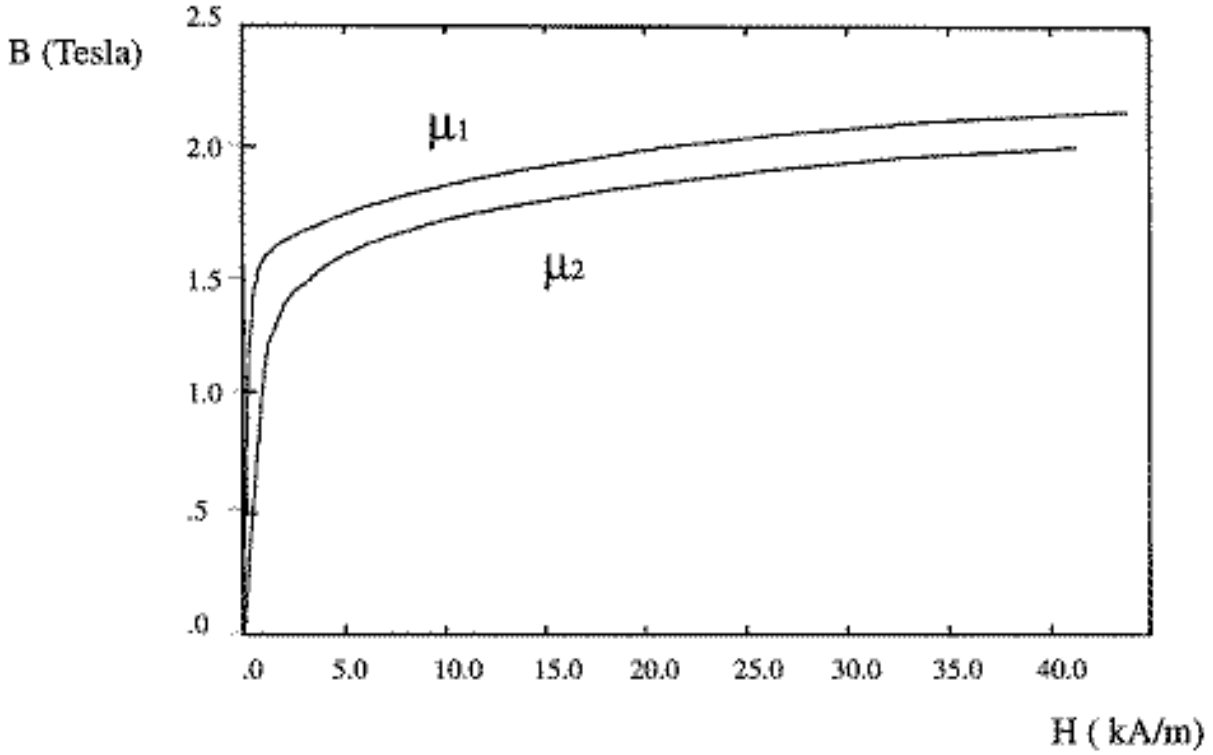

Fig. 6.2: B-H curve of a typical construction steel used for the L3 magnet, showing the maximum and minimum values used to compute forces due to inhomogeneous distribution of the magnetic permeability as explained in Chapt. 6.7.3.

The actual coil (542 turns x 4 layers) has been input as a single turn of radial dimensions R_i = 3.110 m, R_o = 3.340 m and 12.380 m length, with a current of nI = 42.290 10^6 A. This corresponds to an induction of 4 T at the interaction point.

6.3 FIELD MAP AND FORCES GENERATED

The magnetic forces generated in the magnet yoke are very large compared to the gravitational forces, which may be neglected.

Figure 6.3 below shows the flux distribution within a quarter of the domain RZ, taking advantage of the cylindrical symmetry around Z and the transverse symmetry in the plane Z = 0. This clearly shows how the favourable dimensional ratio (length/radius) of the solenoid associated to the magnet yoke allows efficient muon detection and measurement up to a pseudorapidity h of 2.4, as explained in Chapt. 2.

The total magnetic field is shown in Fig. 6.8, p. C-6; the magnetic induction is a fairly constant 4 Tesla within the coil and the innermost section of the endcap yoke, whereas the field in the barrel part of the return yoke and in the outermost disk of the endcap yoke is about 1.7 Tesla as expected. In the nose, and in the innermost section of the thick disks of the endcap, the field is changing direction and its radial component becomes quite large (see Fig. 6.9, p. C-7). The effects of the gaps between the barrel rings are clearly evident.

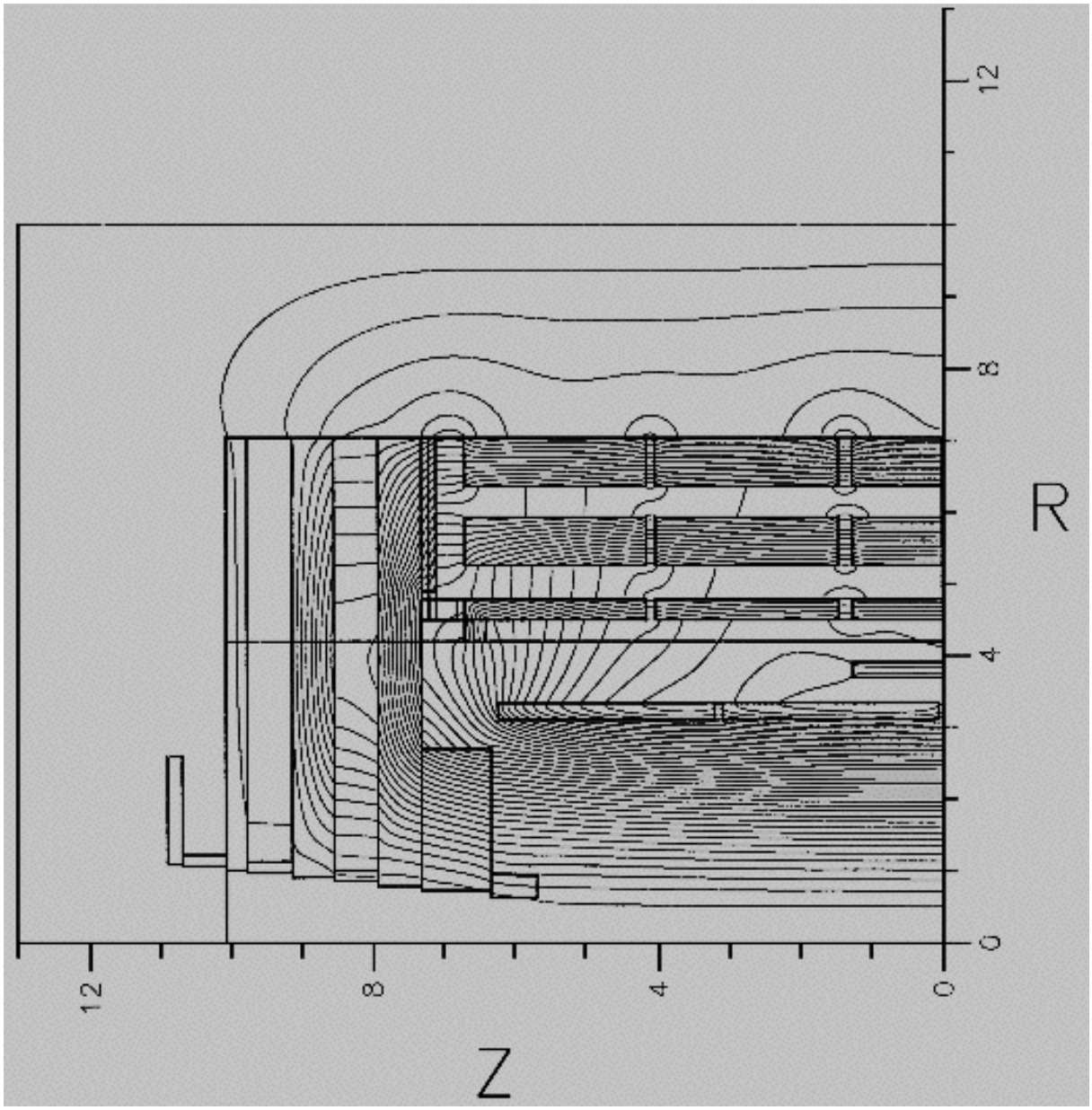

Fig. 6.3: Typical flux line distribution.

The forces generated in the barrel layers and transmitted from ring to ring are quite substantial as shown in Fig. 6.4 below, their main component being in the axial Z direction and pointing inward. They result in compressive axial forces of about 2800 tonnes in the second layer, 3000 tonnes in the third layer, and this requires attention to ensure stability of the barrel ring construction in the Z direction (see Chapt. 7.1.7).

The forces developed on the innermost endcap disk YE1 are also substential. The vector distribution of Maxwell's equivalent surface pressure is shown in Fig. 6.5, and the resulting pressure is plotted in Fig. 8.3 and 8.4.

In general, these forces follow the flux return path, however, the ones pulling the inside edge of the disk toward the interaction point are much stronger than those pulling its outside edge out.

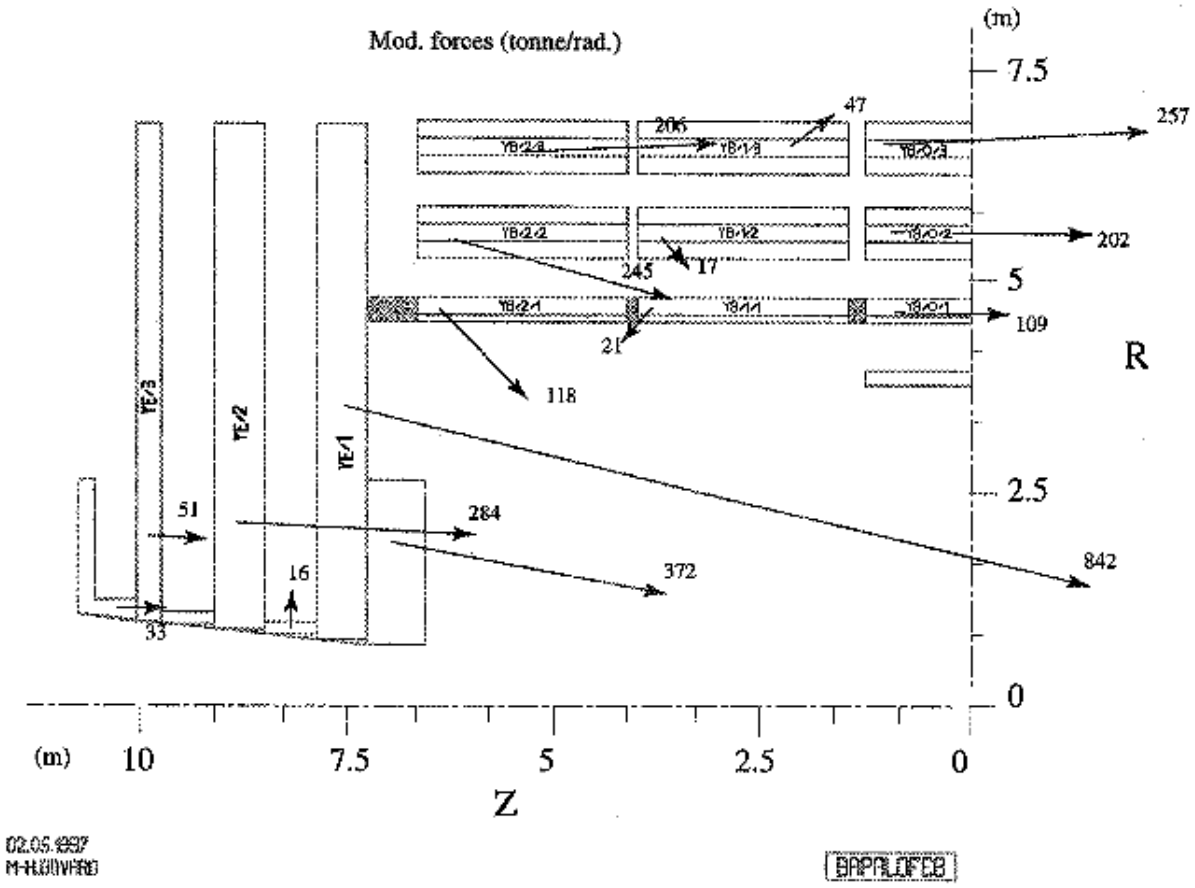

Fig. 6.4: Magnetic forces in tonne/rd acting on the individual elements of the iron yoke, given by POISSON.

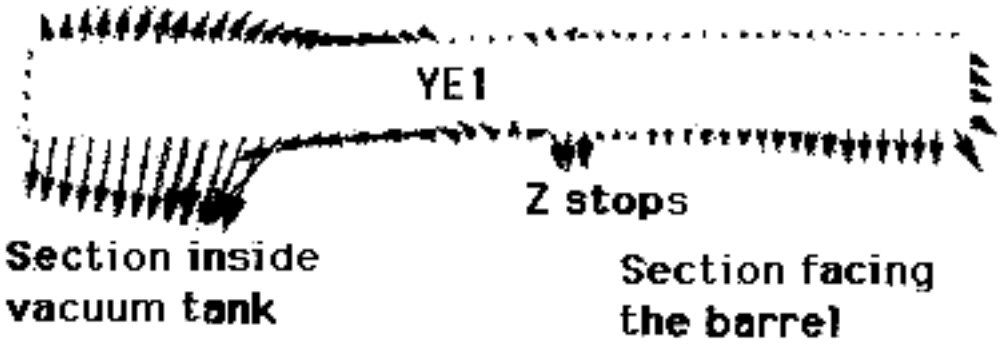

Fig. 6.5: Vector distribution of Maxwell's equivalent surface pressure on YE1.

Table 6.1 shows the total force on each disk and the nose. For both YE1 and the nose YN, this force is roughly a magnitude larger than the gravitational force. The total force of the endcap against the first layer of the barrel rings, transmitted through the Z-stops, is about 8600 tonnes, whereas the total inward pulling force, measured in the central plane, is of the order of 12000 tonnes.

Table 6.1
Magnetic effects on endcap disks.

iron element	YE1	YN	YE2	YE3	total
mass of element (tonne)	706	164	701	347	1918
magnetic force (tonne)	4915	1300	1700	153	8073

The effects of these large forces on the disk construction are fully analysed in Chapt. 8.

6.4 FIELD AT THE DETECTORS AND FIELD MAPPING STRATEGY

Since many of the muon drift chambers will stand in a large magnetic field, both the magnitude and the direction of the field are crucial in determining the correction for each chamber. Despite any possible correction, the field gradient is so important in some areas that it will reduce the expected resolution in the muon chambers (Fig. 6.8, p. C-6 and Fig. 6.9, p. C-7).

A working group has been formed to determine, starting from subdetector performances and physics requirements, the field mapping strategy. In particular the precision to which the field must be known has to be determined for every section, inside of the coil, inside the iron, inside the muon chamber volume etc.

6.5 FIELD AT THE WINDING AND FORCES EXERTED

The current-carrying elements of the superconductor experience both radial and axial forces. Fig. 6.10, p. C-8 shows the distribution of the magnetic induction within the four layers of the coil (for legibility, it should be noted that the layers have been shown separated radially).

Figure 6.6 and Fig. 6.7 given below are respectively showing the axial and radial forces exerted on the coil as a function of distance from the interaction point and/or the Z axis. In this latter case the coil has been implemented in its former four-section modular construction, and it should be noted how the radial force is discontinuous when crossing from one section to the next, thus generating higher shear stresses.

The present magnetic configuration for the monolithic case has been studied in detail and is reported in Chapt. 14.1.1, as it is used as the basis for the mechanical analysis of the coil.

6.6 STRAY FIELD

The stray field has been evaluated to a maximum distance of 50 m with ANSYS at Wisconsin. Fig. 6.11, p. C-9 which incorporates also two close-up views, A and B, for the sake of clarity, gives an idea of what the stray field could be in the UXC5 and USC5 caverns in which most of the electronics will be situated. It is worth noting that, at this stage, the present calculations extend only to 12 m in the Z direction, but they will be extended farther out.

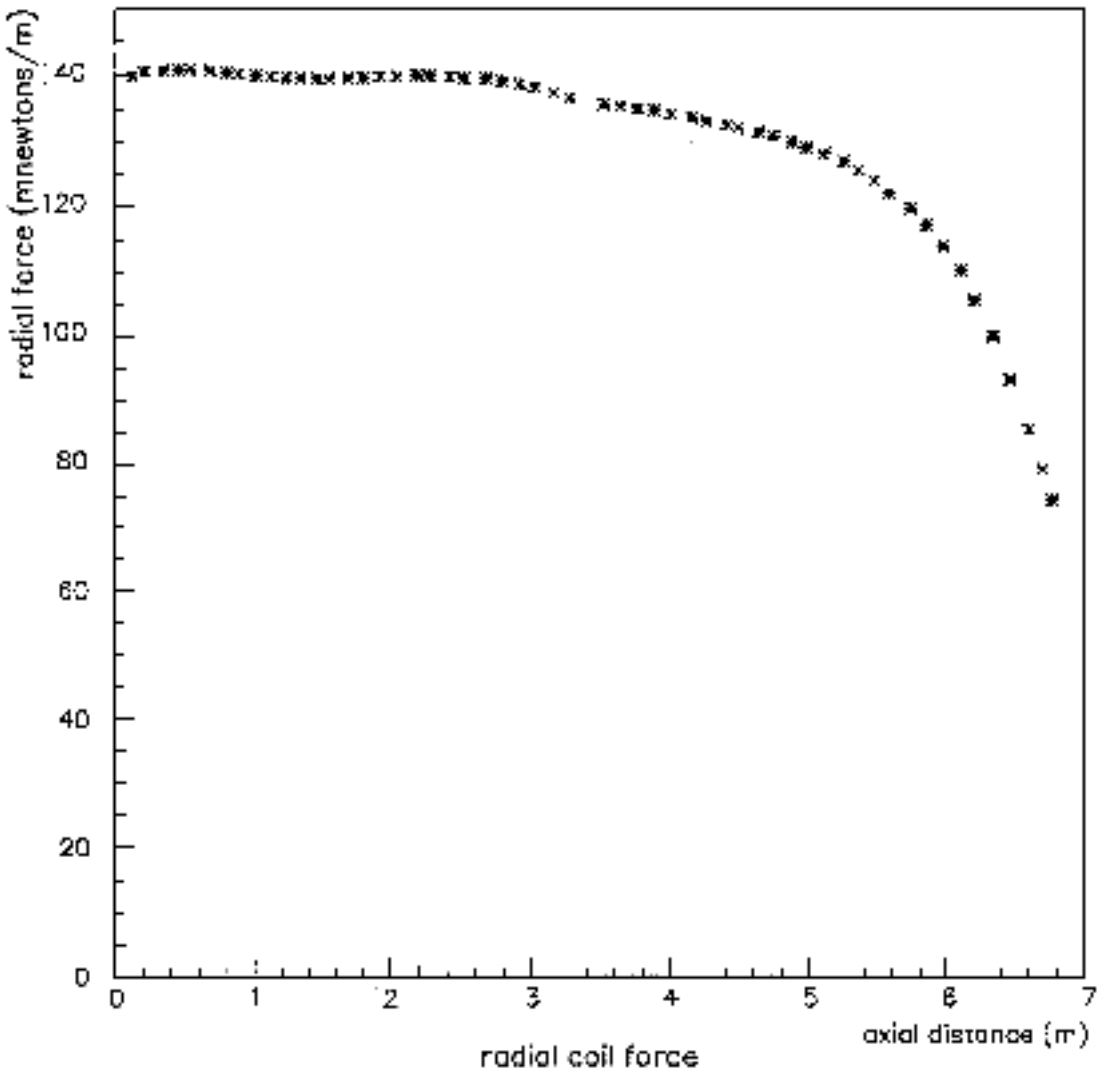

Fig. 6.6: Axial forces in MN/m exerted on the coil.

Generally speaking, the stray field has been found, in the vicinity of the barrel element separations, and at about 1 m distance from the last iron layer, to be of the order of 0.12 T.

This is the area in which some electronic racks will be installed in close proximity on balconies fixed to the magnet yoke, and the presence of this stray field must be fully taken into account from the beginning (see Fig. 26.5, p. C-55 and 26.6, p. C-56).

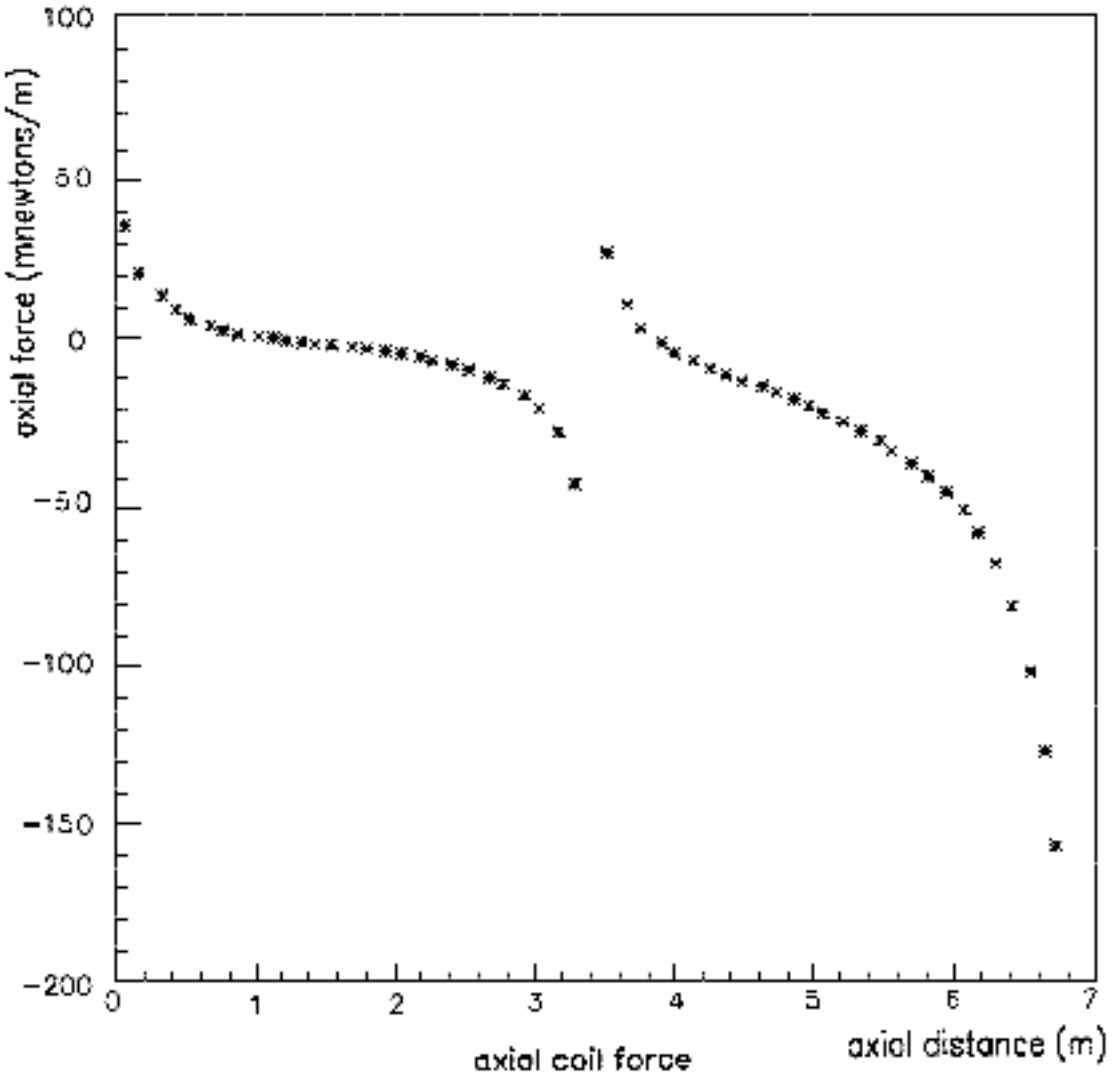

Fig. 6.7: Radial forces in MN/m exerted on the coil.

6.7 3D-FINITE ELEMENT CALCULATIONS

Three dimensional calculations have been performed at CEA Saclay, using the code CASTEM 2000, and at Wisconsin using ANSYS (see also Chapt. 8).

6.7.1 Magnetic forces on the coil due to its misalignment within the iron yoke

Out-of-symmetry displacements of the coil, both off-axis and angular, due to fabrication tolerances and to deformations induced by gravity and by the magnetic field itself may introduce forces and torques acting on the cold mass.

The iron return yoke is considered homogeneous and its non-linear behaviour corresponds to Fig. 6.2.

The resulting axial and radial forces due to axial and radial offsets of the coil of 1, 3 and 10 cm, and resulting torques due to angular tilt of the coil by the same amounts over its half-length, are summarised in Table 6.2 below.

Table 6.2

Forces and torques resulting from axial and radial offset, and from angular tilt of the coil.

axial displacement (cm)	1	3	10
axial force (kN)	840	2540	8140
radial displacement (cm)	1	3	10
radial force (kN)	380	1130	3740
angular tilt (radian / minute)	1/620 ≈ 5.5’	3/620 ≈ 16.5’	10/620 ≈ 55’
torque (kN.m)	2730	8220	27240

These results indicate that the magnetic forces and torques increase linearly with the corresponding displacement, so it will be required to limit the offsets by proper constrainment, the means to reduce them are explained in Chapt. 18.

6.7.2 Magnetic forces on the coil due to asymmetries in the yoke

Whilst both endcap yokes are structurally symmetrical, the barrel yoke has two substantial azimuthal cut outs, to provide passage for the cryogenic and for the electrical and pumping chimneys. The first cut out is a vertical opening traversing the three layers of barrel YB1, with a section of 540 mm x 340 mm in Z for housing a 400 mm diameter conduit. The second one, similarly in barrel YB-1 but at an angle of 30° from the vertical, has a section of 840 mm x 340 mm in Z, for housing an oval conduit 400 mm x 700 mm. The return yoke has been fully modelled in azimuth, and its magnetic behaviour has been taken as uniform. The calculation resulted in a modest force of 2 tonnes, pulling the coil toward the negative Z; the two other components being zero by nature of its symmetry.

Any other asymmetries resulting from the vertical deflection of the barrel rings due to gravity (of second order importance since this does not affect the cross-section of iron offered to the return flux) and from the geometrical tolerances accumulated in assembling the constitutive iron slabs, (expected to be minor and equally distributed in azimuth), have not been taken into consideration.

6.7.3. Magnetic forces on the coil due to inhomogeneous permeability in iron

In the second case, the return yoke is supposed fully symmetrical geometrically but constituted in two halves of different permeabilities m_1 and m_2, as shown in Fig. 6.2.

Two calculations were then carried out: a first one in which the barrel yoke only is affected with two permeabilities; a second one in which both the barrel yoke and the endcap yoke are affected. The result is far more sensitive in the latter case: an order of magnitude larger than in the preceding one. It demonstrates that particular attention should be paid to the endcap disks in which the best homogeneity in permeability must be obtained. Thanks to their construction in sectors (see Chapt. 8), the risk of inhomogeneous permeability will be lessened - if not completely suppressed in the first order – by positioning two sectors coming from the same parent plate into two locations diametrically opposed (see Fig. 8.10) – thus averaging in practice the azimuthal permeability distribution.

The table below summarises these important results.

Table 6.3
Magnetic forces exerted on the coil due to physical asymmetries in the barrel, and to inhomogeneous permeability in the barrel alone and/or in the barrel and endcaps.

condition	Fx (tonne)	Fy (tonne)	Fz (tonne)
physical asymmetries (chimney openings in barrel)	0.	0.	2.
inhomogeneous permeability (in barrel only)	0.	0.	17.
inhomogeneous permeability (both in barrel and endcaps)	0.	0.	102.